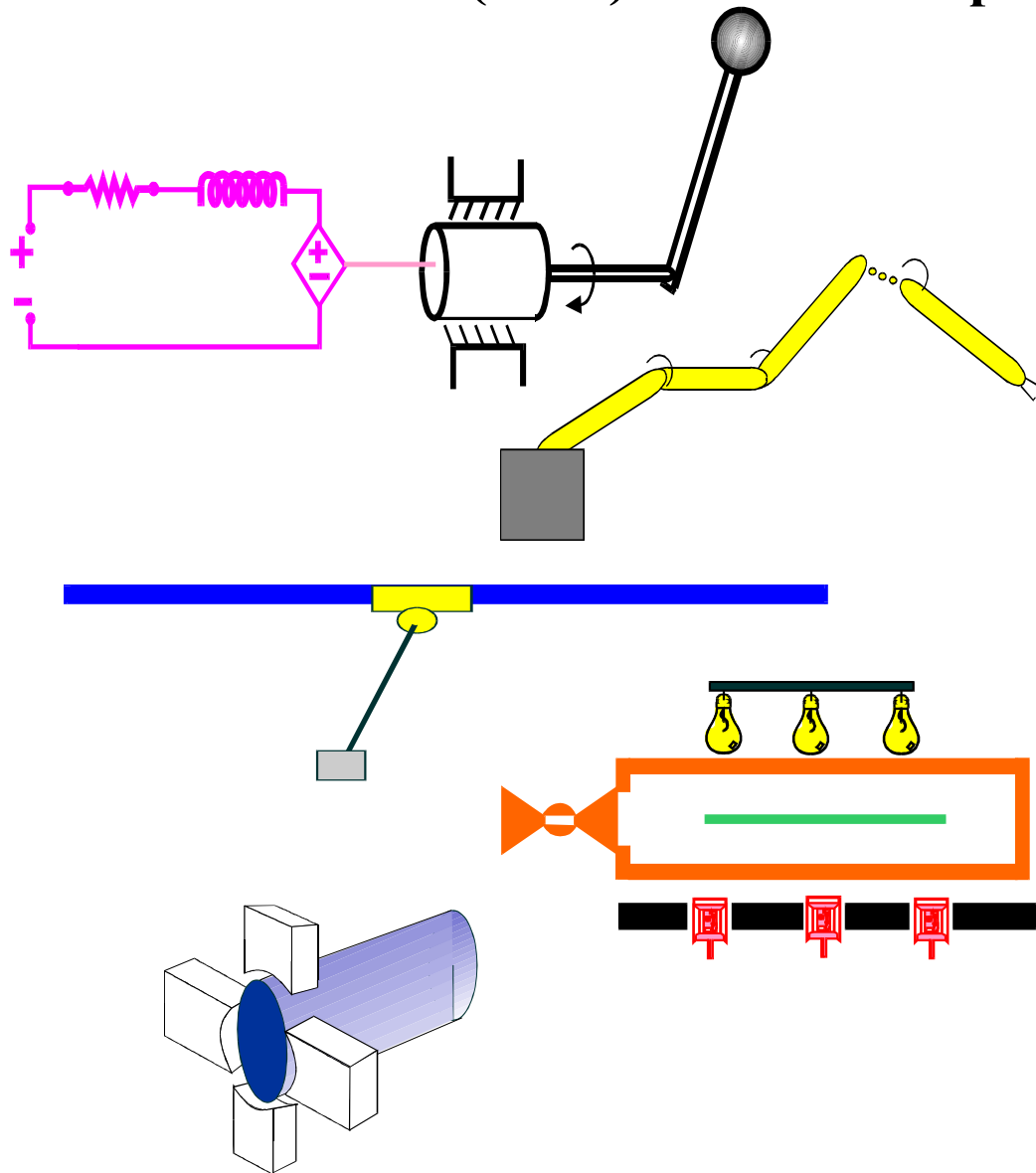# Clemson University
College of Engineering and Science
Control and Robotics (CRB) Technical Report

Number: CU/CRB/5/12/04/#1
Title: Visual Servo Tracking Control of a Wheeled Mobile
Robot with a Monocular Fixed Camera
Authors: J. Chen, W. E. Dixon, D. M. Dawson, and V. K.
Chitrakaran

<table>
<tr><td colspan="2">

Report Documentation Page

</td><td>

</td></tr>
</table>

1. REPORT DATE **2004**	2. REPORT TYPE	3. DATES COVERED **00-00-2004 to 00-00-2004**
4. TITLE AND SUBTITLE **Visual Servo Tracking Control of a Wheeled Mobile Robot with a Monocular Fixed Camera**		5a. CONTRACT NUMBER
		5b. GRANT NUMBER
		5c. PROGRAM ELEMENT NUMBER
6. AUTHOR(S)		5d. PROJECT NUMBER
		5e. TASK NUMBER
		5f. WORK UNIT NUMBER
7. PERFORMING ORGANIZATION NAME(S) AND ADDRESS(ES) **Clemson University,Department of Electrical & Computer Engineering,Clemson,SC,29634-0915**		8. PERFORMING ORGANIZATION REPORT NUMBER
9. SPONSORING/MONITORING AGENCY NAME(S) AND ADDRESS(ES)		10. SPONSOR/MONITOR'S ACRONYM(S)
		11. SPONSOR/MONITOR'S REPORT NUMBER(S)

12. DISTRIBUTION/AVAILABILITY STATEMENT **Approved for public release; distribution unlimited**
13. SUPPLEMENTARY NOTES **The original document contains color images.**
14. ABSTRACT
15. SUBJECT TERMS

16. SECURITY CLASSIFICATION OF:			17. LIMITATION OF ABSTRACT	18. NUMBER OF PAGES	19a. NAME OF RESPONSIBLE PERSON
a. REPORT **unclassified**	b. ABSTRACT **unclassified**	c. THIS PAGE **unclassified**		**11**	

Visual Servo Tracking Control of a Wheeled Mobile Robot with a Monocular Fixed Camera*

J. Chen,[†] W. E. Dixon,[‡] D. M. Dawson,[†] and V. K. Chitrakaran[†]

[†]Department of Electrical & Computer Engineering, Clemson University, Clemson, SC 29634-0915

[‡]Eng. Science and Tech. Div. - Robotics, Oak Ridge National Lab., P.O. Box 2008, Oak Ridge, TN 37831-6305

E-mail: jianc@ces.clemson.edu, dixonwe@ornl.gov, ddawson@ces.clemson.edu, cvilas@ces.clemson.edu

Abstract

In this paper, a visual servo tracking controller for a wheeled mobile robot (WMR) is developed that utilizes feedback from a monocular camera system that is mounted with a fixed position and orientation (i.e., the eye-to-hand problem). A prerecorded image sequence (e.g., a video) of four target points is used to define a desired trajectory for the WMR. By comparing the target points from the prerecorded sequence with the corresponding target points in the live image, projective geometric relationships are exploited to construct a Euclidean homography. The information obtained by decomposing the Euclidean homography is used to develop a kinematic controller. A Lyapunov-based analysis is used to develop an adaptive update law to actively compensate for the lack of depth information required for the translation error system. In contrast to previous WMR visual servo controllers using a fixed camera configuration, the controller in this paper does not require the camera to be mounted so that the optical axis is perpendicular to the WMR plane of motion. An extension is provided to illustrate the development of a visual servo regulation controller. Simulation results are provided to demonstrate the performance of the tracking control design.

1 Introduction

Due to the nonholonomic nature of a wheeled mobile robot (WMR) and the standard encoder hardware configuration (e.g., optical encoders mounted on the actuators), the Euclidean position is difficult to accurately obtain. That is, the linear velocity of the WMR must first be numerically differentiated from the encoder readings (i.e., by the backwards difference algorithm) and then the nonlinear kinematic model must be numerically integrated to obtain the Euclidean position (i.e., dead reckoning).

Since numerical differentiation/integration errors may accumulate over time, it is well known that navigation by dead reckoning is relatively inaccurate. Given recent advances in image extraction/interpretation technology and advances in control theory, an interesting approach to overcome this position measurement problem is to utilize a vision system for navigation.

Motivated by the above discussion, it is clear from a review of literature that numerous researchers have investigated the use of a vision system for WMR navigation. For example, using Extended Kalman Filtering (EKF) techniques on the linearized kinematic model, the authors of [6] used feedback from a monocular omnidirectional camera system to enable wall following, follow-the-leader, and position regulation tasks. Also using EKF techniques, the authors of [13] recently proposed a monocular visual servo tracking controller for WMRs that relies on consecutive image frames and an object database. However, a drawback of the EKF approaches developed in [6] and [13] is the linearization requirement. In [12], Hager et al. used a monocular vision system mounted on a pan-tilt-unit to generate image-Jacobian and geometry-based controllers by using different snapshots of the target and an epipolar constraint. As stated in [1], a drawback of the method developed in [12] is that the system equations become numerically ill-conditioned for large pan angles. Burschka and Hager [1] proposed a vision-based controller for WMRs with a conventional camera and a pan-tilt head or a omnidirectional camera. Drawbacks of the result in [1] include: 1) the requirement for an off-line teaching phase to estimate an object height to allow for an image Jacobian to be (pseudo) inverted, and 2) the WMR controller simply replays the prerecorded linear and angular velocity signals obtained during the teaching phase where the motion of the WMR is restricted to circles and straight lines. In [19], Song and Huang use spatiotemporal apparent velocities obtained from an optical flow of successive images to estimate the depth information for a monocular "guide robot". An optical flow estimation technique was also developed in [14]. However, typical drawbacks of optical flow techniques include the need for temporal smoothing and excessive image processing to determine the image flow; resulting in an intensive computa-

tional burden for real-time robotics control. In [7], Dixon et al. used feedback from an uncalibrated, fixed (ceiling-mounted) camera to develop an adaptive tracking controller for a WMR that compensated for the parametric uncertainty in the camera and the WMR dynamics. Unfortunately, the result in [7] requires that the camera be mounted so that the optical axis is perpendicular with the WMR plane of motion so that the depth from the camera to the robot remains constant. An image-based visual servo controller that exploits an object model was proposed in [20] to solve the WMR tracking controller that adapted for the constant, unknown height of an object moving in a plane through Lyapunov-based techniques.

In contrast to the previous image-based visual servo control approaches, novel homography-based visual servo control techniques (coined 2.5 D visual servoing) have been recently developed (e.g., [2], [3], [15]-[17]). This approach exploits a hybrid combination of reconstructed Euclidean information and image-space information in the control design. The Euclidean information is reconstructed by decoupling the interaction between translation and rotation components of a homography matrix. As stated in [17], some advantages of this methodology over previous image-based approaches are that an accurate Euclidean model of the environment (as in [20]) is not required and potential singularities in the image-Jacobian are eliminated (i.e., the image-Jacobian for homography-based visual servo controllers is typically triangular). In [4], a homography-based adaptive visual servo controller is developed to enable a robot manipulator to track a desired Euclidean-space trajectory as determined by a sequence of images for the fixed camera configuration. In [9], a visual servo controller was developed to asymptotically regulate the position/orientation of a WMR to a constant Euclidean position defined by a reference image, despite unknown depth information where the camera was mounted on-board the WMR. The camera on-board result in [9] was extended in [5] to address the more general tracking problem proposed in [4] for robot manipulators.

In this paper, an adaptive visual servo controller is developed for the off-board, fixed camera configuration that ensures global tracking for a WMR (i.e., the eye-to-hand tracking problem for a WMR). The approach in this paper is based on ideas from our previous results in [4], [5], and [9], since the results in this paper also exploit homography-based techniques. However, the error system development, control design, and stability analysis in this effort requires fundamentally new control approaches in comparison to our result in [4] (which also examines the fixed camera configuration tracking problem) since WMRs are underactuated systems subject to nonholonomic motion constraints (i.e., a typical feedback linearizing controller developed for holonomic systems can not be used to solve the problem, see [8] for further discussion regarding this issue). The results in this paper are also in contrast to [5], where the camera is on-board a WMR. Specifically, new development is required to address the

differences in the open-loop error systems resulting from the geometric differences related to the camera configuration. Moreover, due to the different camera configuration in [5]and [9], the computation of the homography matrix in the present result is more complicated since the image features are not confined to move in a fixed plane. In contrast to our result in [7] (which does not use homography-based approaches), the controller in this paper does not require the camera to be mounted so that the optical axis is perpendicular to the WMR plane of motion (i.e., the depth to the WMR is allowed to be time-varying). To address the fact that the distance from the camera to the WMR is an unknown time-varying signal, a Lyapunov-based control strategy is employed that provides a framework for the construction of an adaptive update law to actively compensate for an unknown depth-related scaling constant. In lieu of tracking a prerecorded set of images, the problem could also be formulated in terms of tracking the desired linear and angular velocities of a reference robot. An extension is provided to illustrate how a visual servo regulation controller can also be designed for the fixed camera configuration. Simulation results are provided to demonstrate the performance of the tracking control design.

2   Problem Formulation

In this paper, the planar motion of a WMR is assumed to be visible by a single camera mounted with a fixed position and orientation[1]. An inertial reference frame, denoted by $\mathcal{I}$, is attached to the camera. The origin of an orthogonal coordinate system $\mathcal{F}$ is coincident with the center of the WMR wheel axis. As illustrated in Figure 1, the xy-axis of $\mathcal{F}$ defines the plane of motion where the x-axis of $\mathcal{F}$ is perpendicular to the wheel axis, and the y-axis is parallel to the wheel axis. The z-axis of $\mathcal{F}$ is perpendicular to the plane of motion and is located at the center of the wheel axis. The linear velocity of the WMR along the x-axis is denoted by $v_c(t) \in \mathbb{R}$, and the angular velocity $\omega_c(t) \in \mathbb{R}$ is about the z-axis of $\mathcal{F}$ (see Figure 1). A desired trajectory is defined by a prerecorded time-varying trajectory of $\mathcal{F}_d$ that is assumed to be second-order differentiable where $v_{cd}(t)$, $\omega_{cd}(t) \in \mathbb{R}$ denote the desired linear and angular velocity of $\mathcal{F}_d$, respectively. A fixed orthogonal coordinate system, denoted by $\mathcal{F}^*$, represents a fixed (i.e., a single snapshot) reference position and orientation of the WMR relative to the fixed camera.

3   Model Development

To facilitate the subsequent development, the WMR is assumed to be identifiable by four feature points denoted by O_i $\forall i = 1, 2, 3, 4$ that are considered to be copla-

---

[1]No assumptions are made with regard to the alignment of the WMR plane of motion and the focal axis of the camera as in [7].

nar[2] and not colinear. It is also assumed that a feature point is located at the origin of the coordinate frame attached to the WMR. Each feature point on $\mathcal{F}$, $\mathcal{F}_d$, and $\mathcal{F}^*$ has a 3D Euclidean coordinate that can be expressed in terms of $\mathcal{I}$, as $\bar{m}_i(t)$, $\bar{m}_{di}(t)$, $\bar{m}_i^* \in \mathbb{R}^3$, respectively. Based on the geometric relationships between the coordinate frames (see Figure 2), the following expressions[3] can be developed to relate the feature points on $\mathcal{F}$ and $\mathcal{F}_d$ to the feature points on $\mathcal{F}^*$

$$
\begin{aligned}
\bar{m}_i &= \left(\bar{R} + \bar{x}_h n^{*T} \right) \bar{m}_i^* \\
\bar{m}_{di} &= \left(\bar{R}_d + \bar{x}_{hd} n^{*T} \right) \bar{m}_i^*.
\end{aligned}
\tag{1}
$$

In (1), $n^* \in \mathbb{R}^3$ denotes the constant unit normal expressed in $\mathcal{I}$ that is perpendicular to the WMR plane of motion, and $\bar{R}(t)$, $\bar{R}_d(t) \in SO(3)$ and $\bar{x}_h(t)$, $\bar{x}_{hd}(t) \in \mathbb{R}^3$ are defined as follows

$$
\begin{aligned}
\bar{R} &\triangleq R\left(R^*\right)^T & \bar{R}_d &\triangleq R_d\left(R^*\right)^T \\
\bar{x}_h &\triangleq x_h - \bar{R}x_h^* & \bar{x}_{hd} &\triangleq x_h - \bar{R}_d x_h^*
\end{aligned}
\tag{2}
$$

where $R(t)$, $R_d(t)$, $R^* \in SO(3)$ denote the rotation from $\mathcal{F}$ to $\mathcal{I}$, $\mathcal{F}_d$ to $\mathcal{I}$, and $\mathcal{F}^*$ to $\mathcal{I}$, respectively, and $x_h(t)$, $x_{hd}(t)$, $x_h^* \in \mathbb{R}^3$ denote the respective scaled translation vectors expressed in $\mathcal{I}$ (See Figure 2). Also in Figure 2, $s_i \in \mathbb{R}^3$ denotes the constant coordinates of the $i-th$ target point, and $d^* \in \mathbb{R}$ denotes the constant distance from the origin of $\mathcal{I}$ to the WMR plane of motion along the normal n^*. From the geometry illustrated in Figure 2, the following relationships can be determined

$$
d^* = n^{*T}\bar{m}_i = n^{*T}\bar{m}_{di}
\tag{3}
$$

where

$$
n^* = R \begin{bmatrix} 0 & 0 & -1 \end{bmatrix}^T = R_d \begin{bmatrix} 0 & 0 & -1 \end{bmatrix}^T.
\tag{4}
$$

The relationship given by (1) provides a means to quantify a translation and rotation error between $\mathcal{F}$ and $\mathcal{F}^*$ and between $\mathcal{F}_d$ and $\mathcal{F}^*$. Since the Euclidean position of $\mathcal{F}$, $\mathcal{F}_d$, and $\mathcal{F}^*$ cannot be directly measured, further development is required to obtain the position and rotational error information in terms of measureable imagespace coordinates. To this end, the normalized Euclidean coordinates of the points on $\mathcal{F}$, $\mathcal{F}_d$, and $\mathcal{F}^*$ expressed in terms of $\mathcal{I}$ as $m_i(t)$, $m_{di}(t)$, $m_i^* \in \mathbb{R}^3$, are defined as follows

$$
m_i \triangleq \frac{\bar{m}_i}{z_i} \qquad m_{di} \triangleq \frac{\bar{m}_{di}}{z_{di}} \qquad m_i^* \triangleq \frac{\bar{m}_i^*}{z_i^*}
\tag{5}
$$

under the standard assumption that the distances from the origin of $\mathcal{I}$ to the target points along the focal axis remains positive (i.e., $z_i(t)$, $z_{di}(t)$, $z_i^* > \varepsilon$ where ε denotes

---

[2]It should be noted that if four coplanar target points are not available then the subsequent development can exploit the classic eight-points algorithm [16] with no four of the eight target points being coplanar.

[3]See [4] for details regarding the development of the following relationships.

an arbitrarily small positive constant). Based on (5), the expression in (1) can be rewritten as follows

$$
m_i = \underbrace{\frac{z_i^*}{z_i}}_{\alpha_i} \underbrace{\left(\bar{R} + \bar{x}_h n^{*T} \right)}_{H} m_i^*
\tag{6}
$$

$$
m_{di} = \underbrace{\frac{z_i^*}{z_{di}}}_{\alpha_{di}} \underbrace{\left(\bar{R}_d + \bar{x}_{hd} n^{*T} \right)}_{H_d} m_i^*
\tag{7}
$$

where $\alpha_i(t)$, $\alpha_{di}(t) \in \mathbb{R}$ denote invertible depth ratios, and $H(t)$, $H_d(t) \in \mathbb{R}^{3\times3}$ denote Euclidean homographies.

Remark 1 *The subsequent development requires that the constant rotation matrix R^* be known. This is a mild assumption since the constant rotation matrix R^* can be obtained a priori using various methods (e.g., a second camera or an additional well-calibrated WMR pose, Euclidean measurements).*

Each target point on $\mathcal{F}$, $\mathcal{F}_d$, and $\mathcal{F}^*$ will also have a projected pixel coordinate expressed in terms of $\mathcal{I}$, denoted by $u_i(t)$, $v_i(t) \in \mathbb{R}$ for $\mathcal{F}$, $u_{di}(t)$, $v_{di}(t) \in \mathbb{R}$ for $\mathcal{F}_d$, and u_i^*, $v_i^* \in \mathbb{R}$ for $\mathcal{F}^*$, that are defined as elements of $p_i(t)$ (i.e., the actual time-varying target points), $p_{di}(t)$ (i.e., the desired time-varying target point trajectory), and p_i^* (i.e., the constant reference target points), respectively. To calculate the Euclidean homography given in (6) and (7) from pixel information, the projected 2D pixel coordinates of the target points are related to $m_i(t)$, $m_{di}(t)$, and m_i^* by the following pin-hole lens models [10]

$$
p_i = Am_i \qquad p_{di} = Am_{di} \qquad p_i^* = Am_i^*
\tag{8}
$$

where $A \in \mathbb{R}^{3\times3}$ is a known, constant, and invertible intrinsic camera calibration matrix. After substituting (8) into (6) and (7), the following relationships can be developed

$$
p_i = \alpha_i \underbrace{\left(AHA^{-1} \right)}_{G} p_i^* \qquad p_{di} = \alpha_{di} \underbrace{\left(AH_d A^{-1} \right)}_{G_d} p_i^*
\tag{9}
$$

where $G(t) = [g_{ij}(t)]$, $G_d(t) = [g_{dij}(t)] \quad \forall i,j = 1,2,3 \in \mathbb{R}^{3\times3}$ denote projective homographies.

From the first relationship in (9), a set of 12 linearly independent equations given by the 4 target point pairs $(p_i^*, p_i(t))$ with 3 independent equations per target point pair can be used to determine the projective homography up to a scalar multiple (i.e., the product $\alpha_i(t)G(t)$ can be determined). From the definition of $G(t)$ given in (9), various techniques can then be used (e.g., see [11], [21]) to decompose the Euclidean homography, to obtain $\alpha_i(t)$, $G(t)$, $H(t)$, and the rotation signal $\bar{R}(t)$. Likewise, by using the target point pairs $(p_i^*, p_{di}(t))$, the desired Euclidean homography can be decomposed to obtain $\alpha_{di}(t)$, $G_d(t)$, $H_d(t)$, and the desired rotation signal $\bar{R}_d(t)$. The rotation matrices $R(t)$ and $R_d(t)$ can be computed

from $\bar{R}(t)$ and $\bar{R}_d(t)$ by using (2) and the fact that R^* is assumed to be known. The normalized coordinates $m_i(t)$ and $m_{di}(t)$ can be computed from $p_i(t)$ and $p_{di}(t)$ by using (8). Hence, $R(t)$, $\bar{R}(t)$, $R_d(t)$, $\bar{R}_d(t)$, $m_i(t)$, $m_{di}(t)$, and the depth ratios $\alpha_i(t)$ and $\alpha_{di}(t)$ are all known signals that can be used for control synthesis.

Based on the definitions for $R(t)$, $R_d(t)$, and R^* provided in the previous development, the rotation from $\mathcal{F}$ to $\mathcal{F}^*$ and from $\mathcal{F}_d$ to $\mathcal{F}^*$, denoted by $R_1(t)$ and $R_{d1}(t)$, are defined as follows

$$R_1 \triangleq R^{*T} R = \begin{bmatrix} \cos\theta & -\sin\theta & 0 \\ \sin\theta & \cos\theta & 0 \\ 0 & 0 & 1 \end{bmatrix} \quad (10)$$

$$R_{d1} \triangleq R^{*T} R_d = \begin{bmatrix} \cos\theta_d & -\sin\theta_d & 0 \\ \sin\theta_d & \cos\theta_d & 0 \\ 0 & 0 & 1 \end{bmatrix} \quad (11)$$

where $\theta(t) \in \mathbb{R}$ denotes the right-handed rotation angle about the z-axis that aligns $\mathcal{F}$ with $\mathcal{F}^*$, and $\theta_d(t) \in \mathbb{R}$ denotes the right-handed rotation angle about the z-axis that aligns $\mathcal{F}_d$ with $\mathcal{F}^*$. From Figure 1 and the definitions of $\theta(t)$ and $\theta_d(t)$, it is clear that

$$\dot{\theta} = \omega_c \qquad \dot{\theta}_d = \omega_{cd} \quad (12)$$

where $\omega_c(t)$ and $\omega_{cd}(t)$ were introduced in Section 2. Based on the fact that $R(t)$, $R_d(t)$, and R^* are known, it is clear from (10)-(12) that $\theta(t)$, $\theta_d(t)$, and $\omega_{cd}(t)$ are known signals that can be used in the subsequent control development. Note that $v_{cd}(t)$ is not a measurable signal. To facilitate the subsequent development, $\theta(t)$ and $\theta_d(t)$ are assumed to be confined to the following regions

$$-\pi < \theta(t) \leqslant \pi \qquad -\pi < \theta_d(t) \leqslant \pi. \quad (13)$$

Remark 2 *Motivation for using a homography-based visual servoing approach is given by the ability to construct the error system in terms of reconstructed Euclidean information and image-space information. As stated in [17], some advantages of this methodology over previous pure image-based approaches are that an accurate Euclidean model of the environment (as in [20]) is not required and potential singularities in the image-Jacobian (which are endemic to traditional pure image-based visual servo controllers) are eliminated (i.e., the resulting image-Jacobian in this paper is always invertible).*

4 Control Development

The control objective in this paper is to ensure that the coordinate frame $\mathcal{F}$ tracks the time-varying trajectory of $\mathcal{F}_d$ (i.e., the Euclidean coordinates of the WMR feature points track the desired time-varying trajectory in the sense that $\bar{m}_i(t) \to \bar{m}_{di}(t)$). To quantify the control objective, the translation and rotation tracking error, denoted by $e(t) \triangleq [e_1(t), e_2(t), e_3(t)]^T \in \mathbb{R}^3$, is defined as

follows

$$\begin{aligned} e_1 &\triangleq \eta_1 - \eta_{d1} \\ e_2 &\triangleq \eta_2 - \eta_{d2} \\ e_3 &\triangleq \theta - \theta_d \end{aligned} \quad (14)$$

where $\theta(t)$ and $\theta_d(t)$ are introduced in (10) and (11), respectively, and the auxiliary signals $\eta(t) \triangleq [\eta_1(t), \eta_2(t), \eta_3]^T$, $\eta_d(t) \triangleq [\eta_{d1}(t), \eta_{d2}(t), \eta_{d3}]^T \in \mathbb{R}^3$ are defined as follows[4]

$$\eta(t) \triangleq \frac{1}{z_1^*} R^T \bar{m}_1 \qquad \eta_d(t) \triangleq \frac{1}{z_1^*} R_d^T \bar{m}_{d1}. \quad (15)$$

From (3), (4), and (15), it can be determined that

$$\eta_3 = \eta_{d3} = \frac{-d^*}{z_1^*}. \quad (16)$$

The expression in (5)-(8) can be used to rewrite $\eta(t)$ and $\eta_d(t)$ in terms of the measurable signals $\alpha_1(t)$, $\alpha_{d1}(t)$, $R(t)$, $R_d(t)$, $p_1(t)$, and $p_{d1}(t)$ as follows

$$\eta(t) = \frac{1}{\alpha_1} R^T A^{-1} p_1 \qquad \eta_d(t) = \frac{1}{\alpha_{d1}} R_d^T A^{-1} p_{d1}. \quad (17)$$

Based on (14), (17), and the fact that $\theta(t)$ and $\theta_d(t)$ are measurable, it is clear that $e(t)$ is measurable. By examining (14)-(16), it can be shown that the control objective is achieved if $\|e(t)\| \to 0$. Specifically, if $e_3(t) \to 0$, then it is clear from (10), (11), and (14) that $R(t) \to R_d(t)$. If $e_1(t) \to 0$ and $e_2(t) \to 0$, then from (14) and (16) it is clear that $\eta(t) \to \eta_d(t)$. Given that $R(t) \to R_d(t)$ and that $\eta(t) \to \eta_d(t)$, then (15) can be used to conclude that $\bar{m}_1(t) \to \bar{m}_{d1}(t)$. If $\bar{m}_1(t) \to \bar{m}_{d1}(t)$ and $R(t) \to R_d(t)$, then (1) can be used to prove that $\bar{m}_i(t) \to \bar{m}_{di}(t)$.

Remark 3 *To develop a tracking controller, it is typical for the desired trajectory to be used as a feedforward component in the control design. Hence, for a kinematic controller the desired trajectory is required to be at least first order differentiable and at least second order differentiable for a dynamic level controller. From the Euclidean homography introduced in (6), $m_d(t)$ can be expressed in terms of the a priori known functions $\alpha_{di}(t)$, $H_d(t)$, $R_d(t)$, and $x_{hd}(t)$. Since these signals can be obtained from the prerecorded sequence of images, sufficiently smooth functions can be generated for these signals by fitting a sufficiently smooth spline function to the signals. Hence, in practice, the a priori developed smooth functions $\alpha_{di}(t)$, $R_d(t)$, and $\eta_d(t)$ can be constructed as bounded functions with sufficiently bounded time derivatives. Given $\theta_d(t)$ and the time derivative of $R_d(t)$, $\dot{\theta}_d(t)$ can be determined. In the subsequent tracking control development, $\dot{\eta}_{d1}(t)$ and $\dot{\theta}_d(t)$ will be used as feedforward control terms.*

---

[4] Any point O_i can be utilized in the subsequent development; however, to reduce the notational complexity, we have elected to select the image point O_1, and hence, the subscript 1 is utilized in lieu of i in the subsequent development.

4.1 Open-loop Error System

To facilitate the development of the open-loop tracking error system, we take the time derivative of (15) as follows

$$\dot{\eta} = \frac{v}{z_1^*} + \left[\eta - \frac{s_1}{z_1^*} \right]_\times \omega \qquad (18)$$

where the following relationships were utilized [4]

$$\dot{m}_1 = Rv + R\left[\omega\right]_\times s_1 \qquad \dot{R} = R\left[\omega\right]_\times \qquad (19)$$

and $v(t)$, $\omega(t) \in \mathbb{R}^3$ denote the respective linear and angular velocity of the WMR expressed in $\mathcal{F}$ as

$$v \triangleq \begin{bmatrix} v_c & 0 & 0 \end{bmatrix}^T \qquad \omega \triangleq \begin{bmatrix} 0 & 0 & \omega_c \end{bmatrix}^T . \qquad (20)$$

In (18), the notation $[\cdot]_\times$ denotes the 3×3 skew-symmetric matrix form of the vector argument.

Without loss of generality, we assume that the feature point O_1 is the feature point assumed to be located at the origin of the coordinate frame attached to the WMR, so that $s_1 = [0, 0, 0]^T$. Based on (20) and the assumption that $s_1 = [0, 0, 0]^T$, we can rewrite (18) as follows

$$\dot{\eta}_1 = \frac{v_c}{z_1^*} + \eta_2 \omega_c \qquad (21)$$
$$\dot{\eta}_2 = -\eta_1 \omega_c .$$

Since the desired trajectory is assumed to be generated in accordance with the WMR motion constraints, a similar expression to (21) can be developed as follows

$$\dot{\eta}_{d1} = \frac{v_{cd}}{z_1^*} + \eta_{d2} \omega_{cd} \qquad (22)$$
$$\dot{\eta}_{d2} = -\eta_{d1} \omega_{cd}.$$

After taking the time derivative of (14) and utilizing (12) and (21), the following open-loop error system can be obtained

$$z_1^* \dot{e}_1 = v_c + z_1^*(\eta_2 \omega_c - \dot{\eta}_{d1})$$
$$\dot{e}_2 = -\eta_1 \omega_c + \eta_{d1} \dot{\theta}_d \qquad (23)$$
$$\dot{e}_3 = \omega_c - \dot{\theta}_d.$$

To facilitate the subsequent development, the auxiliary variable $\bar{e}_2(t) \in \mathbb{R}$ is defined as

$$\bar{e}_2 \triangleq e_2 + \eta_{d1} e_3. \qquad (24)$$

After taking the time derivative of (24) and utilizing (23), the following expression is obtained

$$\dot{\bar{e}}_2 = -e_1 \omega_c + \dot{\eta}_{d1} e_3. \qquad (25)$$

Based on (24), it is clear that if $\bar{e}_2(t)$, $e_3(t) \to 0$, then $e_2(t) \to 0$. Based on this observation and the open-loop dynamics given in (25), the following control development is based on the desire to show that $e_1(t), \bar{e}_2(t), e_3(t)$ are asymptotically driven to zero.

4.2 Closed-Loop Error System

Based on the open-loop error systems in (23) and (25), the linear and angular velocity control inputs for the WMR are designed as follows

$$v_c \triangleq -k_v e_1 + \bar{e}_2 \omega_c - \hat{z}_1^*(\eta_2 \omega_c - \dot{\eta}_{d1}) \qquad (26)$$

$$\omega_c \triangleq -k_\omega e_3 + \dot{\theta}_d - \dot{\eta}_{d1} \bar{e}_2 \qquad (27)$$

where k_v, $k_\omega \in \mathbb{R}$ denote positive, constant control gains, and $\dot{\theta}_d(t)$ and $\dot{\eta}_{d1}(t)$ are generated as described in Remark 3. In (26), the parameter update law $\hat{z}_1^*(t) \in \mathbb{R}$ is generated by the following differential equation

$$\dot{\hat{z}}_1^* = \gamma_1 e_1(\eta_2 \omega_c - \dot{\eta}_{d1}) \qquad (28)$$

where $\gamma_1 \in \mathbb{R}$ is a positive, constant adaptation gain. After substituting the kinematic control signals designed in (26) and (27) into (23), the following closed-loop error systems are obtained

$$z_1^* \dot{e}_1 = -k_v e_1 + \bar{e}_2 \omega_c + \tilde{z}_1^*(\eta_2 \omega_c - \dot{\eta}_{d1})$$
$$\dot{\bar{e}}_2 = -e_1 \omega_c + \dot{\eta}_{d1} e_3 \qquad (29)$$
$$\dot{e}_3 = -k_\omega e_3 - \dot{\eta}_{d1} \bar{e}_2$$

where (25) was utilized, and the depth-related parameter estimation error, denoted by $\tilde{z}_1^*(t) \in \mathbb{R}$, is defined as follows

$$\tilde{z}_1^* \triangleq z_1^* - \hat{z}_1^* . \qquad (30)$$

5 Stability Analysis

Theorem 1 *The control input designed in (26) and (27) along with the adaptive update law defined in (28) ensure asymptotic WMR tracking in the sense that*

$$\lim_{t \to \infty} \|e(t)\| = 0 \qquad (31)$$

provided the time derivative of the desired trajectory satisfies the following condition

$$\lim_{t \to \infty} \dot{\eta}_{d1} \neq 0. \qquad (32)$$

Proof: To prove Theorem 1, the non-negative function $V(t) \in \mathbb{R}$ is defined as follows

$$V \triangleq \frac{1}{2} z_1^* e_1^2 + \frac{1}{2} \bar{e}_2^2 + \frac{1}{2} e_3^2 + \frac{1}{2\gamma_1} \tilde{z}_1^{*2} . \qquad (33)$$

The following simplified expression can be obtained by taking the time derivative of (33), substituting the closed-loop dynamics from (29) into the resulting expression, and then cancelling common terms

$$\dot{V} = -k_v e_1^2 + e_1 \tilde{z}_1^*(\eta_2 \omega_c - \dot{\eta}_{d1}) - k_\omega e_3^2 - \frac{1}{\gamma_1} \tilde{z}_1^* \dot{\hat{z}}_1^*. \qquad (34)$$

After substituting (28) into (34), the following expression can be obtained

$$\dot{V} = -k_v e_1^2 - k_\omega e_3^2 . \qquad (35)$$

From (33) and (35), it is clear that $e_1(t)$, $\bar{e}_2(t)$, $e_3(t)$, $\tilde{z}_1^*(t) \in \mathcal{L}_\infty$ and that $e_1(t)$, $e_3(t) \in \mathcal{L}_2$. Since $\tilde{z}_1^*(t) \in \mathcal{L}_\infty$ and z_1^* is a constant, the expression in (30) can be used to determine that $\hat{z}_1^*(t) \in \mathcal{L}_\infty$. From the assumption that $\eta_{d1}(t)$, $\dot{\eta}_{d1}(t)$, $\eta_{d2}(t)$, $\theta_d(t)$, and $\dot{\theta}_d(t)$ are constructed as bounded functions, and the fact that $\bar{e}_2(t)$, $e_3(t) \in \mathcal{L}_\infty$, the expressions in (14), (24), and (27) can be used to prove that $e_2(t)$, $\eta_1(t)$, $\eta_2(t)$, $\theta(t)$, $\omega_c(t) \in \mathcal{L}_\infty$. Based on the previous development, the expressions in (26), (28), and (29) can be used to conclude that $v_c(t)$, $\dot{\hat{z}}_1^*(t)$, $\dot{e}_1(t)$, $\dot{\bar{e}}_2(t)$, $\dot{e}_3(t) \in \mathcal{L}_\infty$. Based on the fact that $e_1(t)$, $e_3(t)$, $\dot{e}_1(t)$, $\dot{e}_3(t) \in \mathcal{L}_\infty$ and that $e_1(t)$, $e_3(t) \in \mathcal{L}_2$, Barbalat's lemma [18] can be employed to prove that

$$\lim_{t \to \infty} e_1(t), \, e_3(t) = 0 \ . \tag{36}$$

From (36) and the fact that the signal $\dot{\eta}_{d1}(t)\bar{e}_2(t)$ is uniformly continuous (i.e., $\dot{\eta}_{d1}(t)$, $\ddot{\eta}_{d1}(t)$, $\bar{e}_2(t)$, $\dot{\bar{e}}_2(t) \in \mathcal{L}_\infty$), Extended Barbalat's Lemma (see the Appendix) can be applied to the last equation in (29) to prove that

$$\lim_{t \to \infty} \dot{e}_3(t) = 0 \tag{37}$$

and that

$$\lim_{t \to \infty} \dot{\eta}_{d1}(t)\bar{e}_2(t) = 0 \ . \tag{38}$$

If the desired trajectory satisfies (32), then (38) can be used to prove that

$$\lim_{t \to \infty} \bar{e}_2(t) = 0 \ . \tag{39}$$

Based on the definition of $\bar{e}_2(t)$ given in (24), the results in (36) and (39) can be used to conclude that

$$\lim_{t \to \infty} e_2(t) = 0 \tag{40}$$

provided the condition in (32) is satisfied. $\quad\square$

Remark 4 *The condition given in (32) is in terms of the time derivative of the auxiliary vector $\dot{\eta}_{d1}(t)$. For WMR tracking problems, this assumption is typically expressed in terms of the desired linear and angular velocity of the WMR. To gain insight related to how the condition in (32) can be expressed in terms of the desired WMR linear and angular velocities, the expression in (22) can be substituted into (32) to obtain the following condition*

$$\lim_{t \to \infty} \frac{v_{cd}}{z_1^*} \neq -\eta_{d2}\omega_{cd}. \tag{41}$$

The condition in (41) is comparable to typical WMR tracking results that restrict the desired linear and angular velocity. For an in-depth discussion of this type of restriction including related previous results see [8].

Remark 5 *For some cases, the signals $v_{cd}(t)$ and $\omega_{cd}(t)$ may be a priori known. For this case (12) and (22) can be substituted into (23) as follows*

$$\begin{aligned} z_1^*\dot{e}_1 &= v_c - v_{cd} + z_1^*(\eta_2\omega_c - \eta_{d2}\omega_{cd}) \\ \dot{e}_2 &= -\eta_1\omega_c + \eta_{d1}\omega_{cd} \\ \dot{e}_3 &= \omega_c - \omega_{cd}. \end{aligned} \tag{42}$$

Based on (42), the linear and angular velocity kinematic control inputs for the WMR are redesigned as follows

$$v_c \triangleq -k_v e_1 + v_{cd} + \hat{z}_1^*(\eta_{d2}\omega_{cd} + \bar{e}_2\omega_c - \eta_2\omega_c) \tag{43}$$

$$\omega_c \triangleq -k_\omega e_3 + \omega_{cd} - \bar{e}_2 v_{cd} - \hat{z}_1^*\eta_{d2}\bar{e}_2\omega_{cd} \tag{44}$$

along with the following adaptation law

$$\dot{\hat{z}}_1^* \triangleq -\gamma_1 \left(e_1(\eta_{d2}\omega_{cd} + \bar{e}_2\omega_c - \eta_2\omega_c) - e_3\bar{e}_2\eta_{d2}\omega_{cd} \right). \tag{45}$$

By using the following nonnegative function

$$V_1 \triangleq \frac{1}{2}z_1^* e_1^2 + \frac{1}{2}z_1^*\bar{e}_2^2 + \frac{1}{2}e_3^2 + \frac{1}{2\gamma_1}\tilde{z}_1^{*2} \ , \tag{46}$$

the result in Theorem 1 can also be obtained via (43)-(45).

6 Regulation Extension

Based on the assumption given in (32) and (41), it is clear that the controller developed in the previous section can not be applied to solve the regulation problem. In this section, an extension is presented to illustrate how a visual servo controller can be developed to solve the regulation problem for the fixed camera configuration. To this end, the following kinematic model is obtained by examining Figure 1

$$\begin{bmatrix} \dot{x}_c \\ \dot{y}_c \\ \dot{\theta} \end{bmatrix} = \begin{bmatrix} \cos\theta & 0 \\ \sin\theta & 0 \\ 0 & 1 \end{bmatrix} \begin{bmatrix} v_c \\ \omega_c \end{bmatrix} \tag{47}$$

where $\dot{x}_c(t)$, $\dot{y}_c(t)$, and $\dot{\theta}(t)$ denote the time derivative of $x_c(t)$, $y_c(t)$, and $\theta(t) \in \mathbb{R}$, respectively, where $x_c(t)$ and $y_c(t)$ denote the planar position of $\mathcal{F}$ expressed in $\mathcal{F}^*$, $\theta(t)$ was introduced in (10), and $v_c(t)$ and $\omega_c(t)$ denote the linear and angular velocity of $\mathcal{F}$. In addition to the kinematic model in (47), the geometric relationships between the coordinate frames (see Figure 2), can be used to develop the following expressions[5]

$$\bar{m}_1^* = d^* x_h^* + R^* s_1 \qquad \bar{m}_1 = d^* x_h + R s_1 \tag{48}$$

$$\begin{bmatrix} x_c & y_c & 0 \end{bmatrix}^T = d^* R^{*T} (x_h - x_h^*). \tag{49}$$

After utilizing (5), (48), (49), and the assumption that $s_1 = [0, 0, 0]^T$, the following expression can be obtained

$$\frac{1}{z_1^*} \begin{bmatrix} x_c & y_c & 0 \end{bmatrix}^T = R^{*T} \left[\frac{1}{\alpha_1} m_1 - m_1^* \right] \tag{50}$$

where $\alpha_1(t)$ was defined in (6). After utilizing (8), the expression in (50) can be rewritten as follows

$$\frac{1}{z_1^*} \begin{bmatrix} x_c & y_c & 0 \end{bmatrix}^T = R^{*T} A^{-1} \left[\frac{1}{\alpha_1} p_1 - p_1^* \right]. \tag{51}$$

---

[5] See [4] for details regarding the development of the following relationships.

To facilitate the subsequent control objective, a global invertible transformation is defined as follows [8]

$$
\begin{bmatrix} e_1 \\ e_2 \\ e_3 \end{bmatrix} \triangleq \begin{bmatrix} \cos\theta & \sin\theta & 0 \\ -\sin\theta & \cos\theta & 0 \\ 0 & 0 & 1 \end{bmatrix} \begin{bmatrix} \frac{x_c}{z_1^*} \\ \frac{y_c}{z_1^*} \\ \theta \end{bmatrix} \qquad (52)
$$

where $e(t) = [\ e_1(t)\ \ e_2(t)\ \ e_3(t)\ ]^T \in \mathbb{R}^3$ denotes the regulation error signal. From (10), (51), and (52), it is clear that $e(t)$ is a measurable signal, and that if $\|e(t)\| \to 0$, then $x_c(t) \to 0$, $y_c(t) \to 0$, and $\theta(t) \to 0$. After taking the time derivative of (52), the following open-loop error system can be obtained

$$
\begin{bmatrix} \dot{e}_1 \\ \dot{e}_2 \\ \dot{e}_3 \end{bmatrix} = \begin{bmatrix} \frac{v_c}{z_1^*} + \omega_c e_2 \\ -\omega_c e_1 \\ \omega_c \end{bmatrix} \qquad (53)
$$

where (47) was utilized. Based on (53), the linear and angular velocity inputs are designed as follows

$$
v_c \triangleq -k_1 e_1 \qquad \omega_c \triangleq -k_2 e_3 + e_2^2 \sin t \qquad (54)
$$

to yield the following closed-loop error system

$$
\begin{aligned}
z_1^* \dot{e}_1 &= -k_1 e_1 + z_1^* \omega_c e_2 \\
\dot{e}_2 &= -\omega_c e_1 \\
\dot{e}_3 &= -k_2 e_3 + e_2^2 \sin t.
\end{aligned} \qquad (55)
$$

Theorem 2 *The control input designed in (54) ensures asymptotic WMR regulation in the sense that*

$$
\lim_{t \to \infty} \|e(t)\| = 0. \qquad (56)
$$

Proof: Let $V(t) \in \mathbb{R}$ denote the following non-negative function

$$
V \triangleq \frac{1}{2} z_1^* \left(e_1^2 + e_2^2 \right). \qquad (57)
$$

After taking the time derivative of (57) and utilizing (55), the following simplified expression is obtained

$$
\dot{V} = -k_1 e_1^2. \qquad (58)
$$

By utilizing Barbalat's Lemma and Extended Barbalat's Lemma in a similar manner as in the proof for Theorem 1, the control inputs can be proven to be bounded, and the result in (56) can be obtained [8]. $\square$

7 Simulation Results

A numerical simulation performed to illustrate the performance of the controller given in (26)-(28). The desired trajectory was generated by numerically integrating (22), where the unknown constant scaling term d^* and the desired linear and angular velocity were selected as follows

$$
d^* = 7.86 \text{ [m]} \qquad v_{cd}(t) = 0.2\sin(t) \text{ [m/sec]} \qquad \omega_{cd}(t) = 0.1\sin(t) \text{ [rad/sec]}. \qquad (59)
$$

For the simulation, desired pixel information from a prerecorded sequence of images (and the corresponding spline function) were not utilized to generate the feedforward signals in (26) - (28); rather, (12) and (22) were utilized to calculate $\eta_d(t)$, $\dot{\eta}_{d1}(t)$, $\theta_d(t)$, and $\dot{\theta}_d(t)$. Specifically, by numerically integrating (22) with the values given in (59), the desired signals, denoted by $\eta_{d1}(t)$ and $\eta_{d2}(t)$, can be determined. By numerically integrating $\omega_{cd}(t)$, the value for $\theta_d(t)$ can also be determined. For the simulation, the reference and initial pixels were selected as follows

$$
\begin{aligned}
p_1^* &= [146 \quad 145 \quad 1] \qquad (60) \\
p_1(0) &= [67 \quad 181 \quad 1].
\end{aligned}
$$

Based on the initial condition and reference coordinates in (60), the initial translation and rotation errors were determined as follows

$$
e_1(0) = 0.042 \quad e_2(0) = -0.194 \quad e_3(0) = 1.40 \text{ (rad)}
$$

where

$$
\begin{aligned}
\eta(0) &= [0.140 \quad -0.038 \quad -0.983] \\
\eta_d(0) &= [0.098 \quad 0.156 \quad -0.983].
\end{aligned}
$$

The control gains k_v and k_ω were adjusted to the following values to yield the best performance

$$
k_v = 10 \quad k_\omega = 5.
$$

After the best performance that could be achieved by adjusting the feedback gains was obtained, the adaptation gain γ_1 was adjusted to the following value to yield improved performance

$$
\gamma_1 = 745.
$$

The resulting translational and rotational errors for the WMR are depicted in Figure 3, and the parameter estimate signal is depicted in Figure 4. The control input velocities $v_c(t)$ and $\omega_c(t)$ defined in (26) and (27) are depicted in Figure 5. Note that the angular velocity input was artificially saturated between $\pm 80.25 [\deg \cdot s^{-1}]$.

8 Conclusions

In this paper, the position/orientation of a WMR is forced to track a desired time-varying trajectory defined by a prerecorded sequence of images. To achieve the result, multiple views of four target points were used to develop Euclidean homographies. By decomposing the Euclidean homographies into separate translation and rotation components, reconstructed Euclidean information was obtained for the control development. A Lyapunov-based stability argument was used to design an adaptive update law to compensate for an unknown depth parameter. The impact that the development in this paper makes is that a new analytical approach has been developed using homography-based concepts to enable the

position/orientation of a WMR subject to nonholonomic constraints to track a desired trajectory generated from a sequence of images, despite the lack of depth measurements. In contrast to the work in [7], the camera is not required to be mounted so that the optical axis is perpendicular to the WMR plane of motion. An extension is provided to illustrate the development of a visual servo regulation controller. Simulation results are provided to demonstrate the performance of the tracking control design.

References

[1] D. Burschka and G. Hager, "Vision-Based Control of Mobile Robots," *Proc. of the IEEE International Conference on Robotics and Automation*, pp. 1707-1713, 2001.

[2] F. Chaumette and E. Malis, "2 1/2 D Visual Servoing: A Possible Solution to Improve Image-based and Position-based Visual Servoings," *Proc. of the IEEE International Conference on Robotics and Automation*, pp. 630-635, 2000.

[3] F. Chaumette, E. Malis, and S. Boudet, "2D 1/2 Visual Servoing with Respect to a Planar Object," *Proc. of the Workshop on New Trends in Image-Based Robot Servoing*, pp. 45-52, 1997.

[4] J. Chen, D. M. Dawson, W. E. Dixon, and A. Behal, "Adaptive Homography-Based Visual Servo Tracking", *Proceedings of the 2003 IEEE International Conference on Intelligent Robots and Systems*, Las Vegas, Nevada, October 2003, pp. 230-235.

[5] J. Chen, W. E. Dixon, D. M. Dawson, and M. McIntire, "Homography-based Visual Servo Tracking Control of a Wheeled Mobile Robot", *Proceedings of the 2003 IEEE International Conference on Intelligent Robots and Systems*, Las Vegas, Nevada, October 2003, pp. 1814-1819.

[6] A. K. Das, et al., "Real-Time Vision-Based Control of a Nonholonomic Mobile Robot," *Proc. of the IEEE International Conference on Robotics and Automation*, pp. 1714-1719, 2001.

[7] W. E. Dixon, D. M. Dawson, E. Zergeroglu, and A. Behal, "Adaptive Tracking Control of a Wheeled Mobile Robot via an Uncalibrated Camera System," *IEEE Transactions on Systems, Man, and Cybernetics -Part B: Cybernetics*, Vol. 31, No. 3, pp. 341-352, 2001.

[8] W. E. Dixon, D. M. Dawson, E. Zergeroglu and A. Behal, *Nonlinear Control of Wheeled Mobile Robots*, Springer-Verlag London Limited, 2001.

[9] Y. Fang, D. M. Dawson, W. E. Dixon, and M. S. de Queiroz, "2.5D Visual Servoing of Wheeled Mobile Robots," *Conference on Decision and Control,* Las Vegas, NV, pp. 2866-2871, Dec. 2002.

[10] O. Faugeras, *Three-Dimensional Computer Vision*, The MIT Press, Cambridge Massachusetts, 2001.

[11] O. Faugeras and F. Lustman, "Motion and Structure From Motion in a Piecewise Planar Environment", *International Journal of Pattern Recognition and Artificial Intelligence,* Vol. 2, No. 3, pp. 485-508, 1988.

[12] G. D. Hager, D. J. Kriegman, A. S. Georghiades, and O. Ben-Shahar, "Toward Domain-Independent Navigation: Dynamic Vision and Control," *Proc. of the IEEE Conference on Decision and Control*, pp. 3257-3262, 1998.

[13] B. H. Kim, et al., "Localization of a Mobile Robot using Images of a Moving Target," *Proc. of the IEEE International Conference on Robotics and Automation*, pp. 253-258, 2001.

[14] Y. Ma, J. Kosecka, and S. Sastry, "Vision Guided Navigation for Nonholonomic Mobile Robot", *IEEE Trans. on robotics and Automation*, Vol. 15, No. 3, pp. 521-536, June 1999.

[15] E. Malis and F. Chaumette, "Theoretical Improvements in the Stability Analysis of a New Class of Model-Free Visual Servoing Methods," *IEEE Transactions on Robotics and Automation*, Vol. 18, No. 2, pp. 176-186, April 2002.

[16] E. Malis and F. Chaumette, "2 1/2 D Visual Servoing with Respect to Unknown Objects Through a New Estimation Scheme of Camera Displacement," *International Journal of Computer Vision*, Vol. 37, No. 1, pp. 79-97, June 2000.

[17] E. Malis, F. Chaumette, and S. Bodet, "2 1/2 D Visual Servoing," *IEEE Transactions on Robotics and Automation*, Vol. 15, No. 2, pp. 238-250, April 1999.

[18] J. J. E. Slotine and W. Li, *Applied Nonlinear Control*, Prentice Hall, Inc: Englewood Cliff, NJ, 1991.

[19] K.-T. Song and J.-H. Huang, "Fast Optical Flow Estimation and Its Application to Real-time Obstacle Avoidance," *Proc. of the IEEE International Conference on Robotics and Automation*, pp. 2891-2896, 2001.

[20] H. Y. Wang, S. Itani, T. Fukao, and N. Adachi, "Image-Based Visual Adaptive Tracking Control of Nonholonomic Mobile Robots", *Proc. of the IEEE/RJS International Conference on Intelligent Robots and Systems*, pp. 1-6, 2001.

[21] Z. Zhang and A. R. Hanson, "Scaled Euclidean 3D Reconstruction Based on Externally Uncalibrated Cameras," *IEEE Symp. on Computer Vision*, pp. 37-42, 1995.

Appendix

The Extended Barbalat's Lemma was utilized in the stability analysis for Theorem 1. This lemma stated as follows, and a proof for the Lemma can be found in [8].

Lemma 1 *If a differentiable function $f(t) \in \mathbb{R}$ has a finite limit as $t \to \infty$, and its time derivative can be written as follows*

$$\dot{f}(t) = g_1(t) + g_2(t), \tag{61}$$

where $g_1(t)$ is a uniformly continuous function and

$$\lim_{t \to \infty} g_2(t) = 0, \tag{62}$$

then

$$\lim_{t \to \infty} \dot{f}(t) = 0 \qquad and \qquad \lim_{t \to \infty} g_1(t) = 0. \tag{63}$$
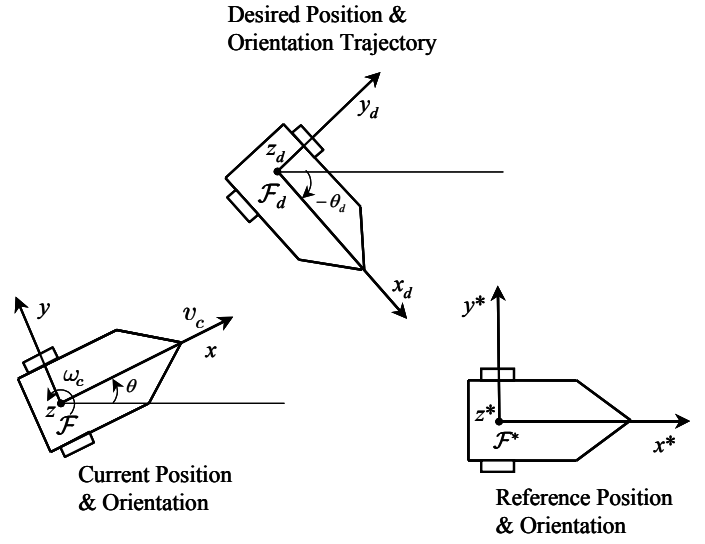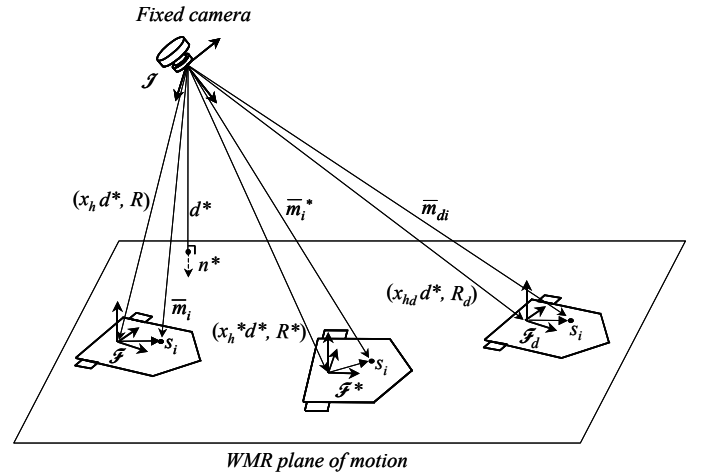

Figure 1: Mobile robot coordinate systems.

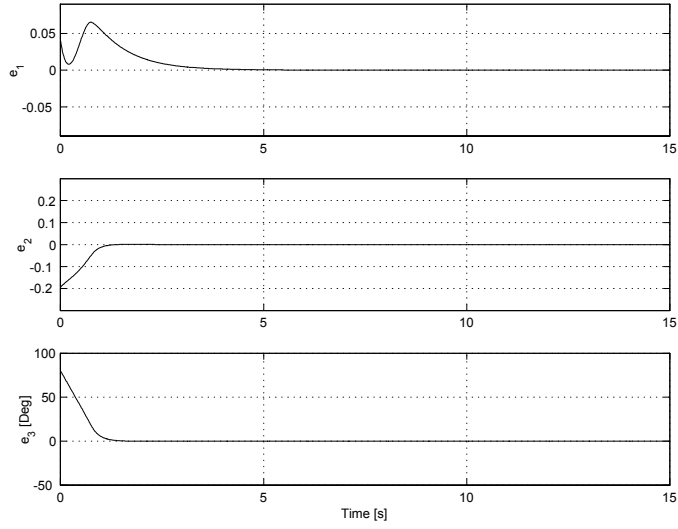Figure 2: WMR coordinate frame relationships.

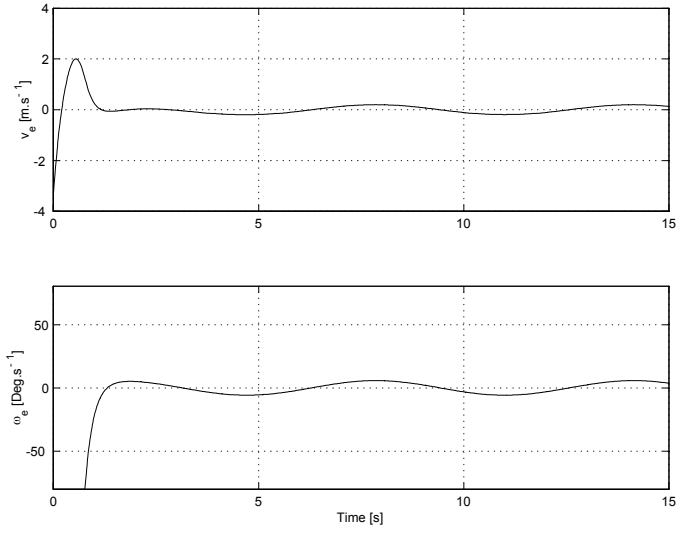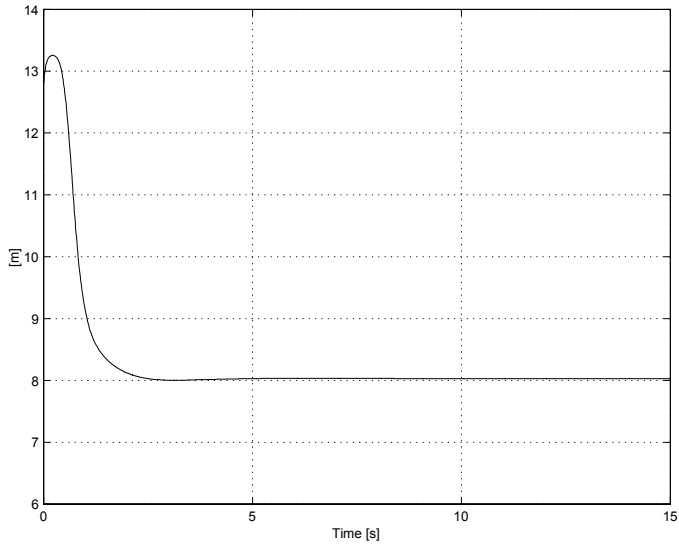Figure 3: Translational and rotational tracking errors.

Figure 5: Linear and angular velocity control inputs.

Figure 4: Parameter estimate.